Emission control in broad periodic waveguides and critical coupling

Henri Benisty, Omer Khayam, Cyril Cambournac

Emission control in broad periodic waveguides and critical coupling

Henri Benisty *, Omer Khayam, Cyril Cambournac

Laboratoire Charles Fabry de l'Institut d'Optique, CNRS, Univ. Paris-Sud, Campus Polytechnique, RD 128, 91127 Palaiseau Cedex, France

Broad periodic channel waveguides, with a corrugation on their edge, exhibit a remarkable structure in their dispersion diagram, in the form of stripes of minigaps, whose hyperbolic shape is demonstrated. Around the Brillouin zone edge, the contra-directional feedback borrows the geometry of Littrow diffraction. Spontaneous emission from a large subset of modes then acquires a strong modulation. Lasing on these modes, the so-called ''Littrow lasing'', offers also the lowest lasing threshold of the open resonator system. Reviewing our recent studies of this system, we discuss slow light and critical coupling phenomena: for a properly adjusted contra-directional coupling, the bands become substantially flat in a sizable area of the dispersion diagram, opening various perspectives. The band engineering tools to master these phenomena and the physical implications in other domains are briefly reviewed.

Keywords: Waveguides; Photonic crystal; Laser; Open resonator; Slow light; Coupled-mode theory

1. Introduction

Confinement of light amounts to design shapes for given materials, based on the properties of the resulting electromagnetic field solutions. Waveguides represent a wide part of the proposed designs. Based on the justified belief that the strongest confinement is associated with the single-mode regime in a waveguide, it might be thought that studying a multimode waveguide is of little use, insofar as the naively expected trend is some sort of averaging among all modes. As we shall see, this is not the case, or not with a $1/N$ scaling (for N modes). To this end, in this paper, we summarize numerous aspects of a periodic multimode waveguide where a rich structure emerges, based on several previous investigations [1–5]. The main results are the formation rules for ''minigap stripe'', and the strong collective slow-down that can be engineered for a substantial fraction of the photonic dispersion diagram of the waveguide modes.

We focus on a quasi-one-dimensional confinement, with one propagating dimension (z), a second dimension (x) which defines a ''broad'' waveguide, and a strongly confined ''frozen'' dimension (y), not considered further. By ''broad'' we mean here that there is a bulk region in the waveguide, where the majority of the intensity profile is confined, with only a modest fraction in the cladding regions, typically at the wavelength scale. A multimode behavior with several similar dispersion branches $\omega(k_z)$ holds for a perfectly z-invariant guide. Here, we study a z-periodic waveguide in this regime: we typically consider photonic crystal (PhC) waveguides where a two-dimensional PhC serves as a cladding, Fig. 1(a), or simply waveguides with edge corrugation, Fig. 1(b). For a PhC waveguide, and for

* Corresponding author. Tel.: +33 1 6453 3286; fax: +33 1 6453 3318.

E-mail address: henri.benisty@institutoptique.fr (H. Benisty).

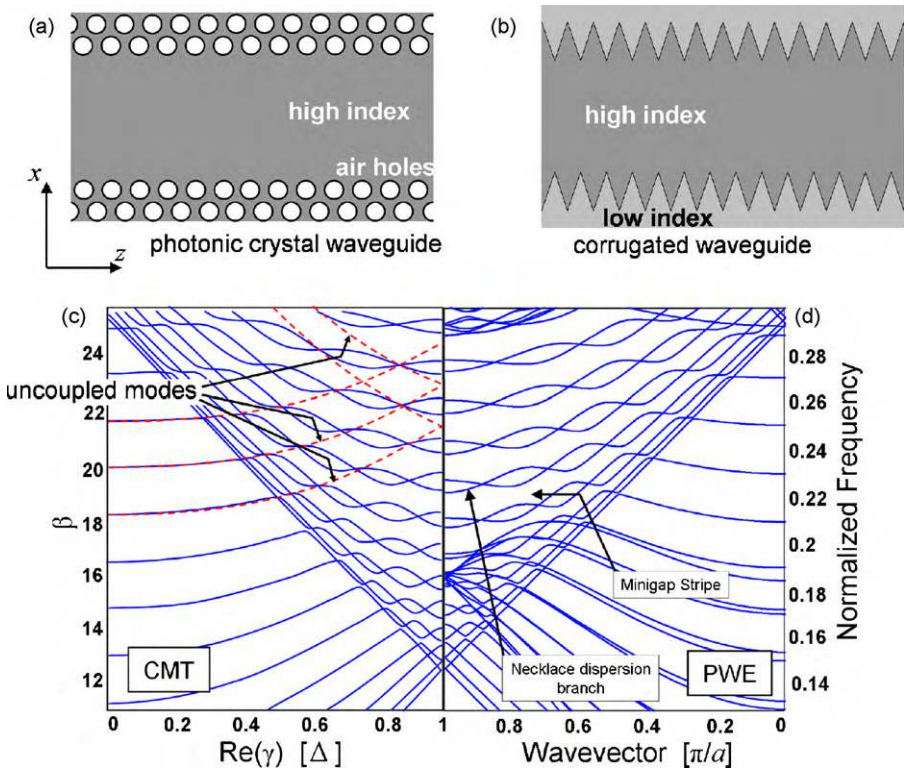

Fig. 1. A broad photonic crystal waveguide (a), and a corrugated waveguide (b); (c) CMT bandstructure calculation based on uncoupled modes and exact calculation for a W15 PhC waveguide.

branches at frequencies within the PhC bandgap, forbidden propagation in the cladding ensures that the modal intensity is mostly concentrated in the bulk part. The PhC waveguide terminology — ''Wn'' for a waveguide made by omitting n missing dense rows in a lattice, will be used [6–8]. We refer to air hole type PhCs, where the triangular lattice provides the best confinement in TE polarization.

In this framework, we may define waveguide modes of an equivalent nonperiodic structure. They then serve as the basis for a Coupled Mode Theory (CMT) approach [9]. We describe the result of this strategy and the formation of minigap stripes in the next part (Section 2). A resulting modulation of density-of-states within a fraction of the Brillouin zone is then evidenced. In Section 3, we describe how our waveguides form ''Littrow resonators'' that offer a privileged avenue for broad-area low-threshold laser systems. In Section 4, the emergence of collective slow light around a particular value of the CMT coupling parameter κ is briefly reviewed, introducing the concept of ''critical coupling''. Its applications either to PhC or to simple edge-corrugated dielectric waveguides are discussed.

2. Broad periodic waveguide modal structure: "stripes of minigap"

Consider a basic dielectric waveguide made of refractive index n and of width W and axis z. Guided branches of its dispersion diagram $\omega(\kappa)$ lie between the lines $kc/n_{\mathrm{cald}} > \omega(\kappa) > kc/n$, with $k \equiv k_z$, and n_{cald} a cladding refractive index. For a perfect metal cladding, the simple relations $\omega_m = (c/n)[k^2 + (m\pi/W)^2]^{1/2}$ holds for the angular frequency of the m-th branch, the field, approximated as scalar, being $E_m^{\pm}(x,z) = \exp(\pm jkz)\sin(m\pi x/W)$.

In the spirit of CMT, a counter-propagating coupling scheme between $E_m^{+}(x,z)$ and $E_m^{-}(x,z)$ branches can be introduced to take into account the effect of periodicity [1,4]. It essentially reads:

$$\frac{\partial F_m^{\pm}}{\partial z} = j\delta_m^{\pm} F_m^{\pm} + \sum_{m'=1,\ldots,N} s_{mm'}\kappa_{mm'} F_{m'}^{\mp} \qquad (1)$$

where $F_m^{\pm}$ are envelope functions for the field amplitudes solutions, thus written as $E_m^{\pm}(x,z) = F_m^{\pm}(z)\exp(\pm jKz)\sin(m\pi x/W)$. In this expression, the wavevector $K = K_{\mathrm{BZE}} \equiv \pi/a$ is the Brillouin zone edge (BZE) for a

guide of period a, half the Bragg wavevector. Accordingly, the detuning terms $\delta_m^{\pm}$ incorporate the wavevector difference. Without any coupling, the $\exp(j\delta_m^{\pm}z)$ evolution of $F_m^{\pm}$ implies that $\delta_m^{\pm} \pm K = \pm k(\omega_m)$ which defines the m-th detuning as a function of ω and notably contains its relation with the group velocity of the uncoupled mode $v_m^g = \partial\omega_m/\partial k$. Here v_m^g varies, without coupling, from 0 at $k = 0$, to (c/n) asymptotically. As for the coupling terms; $s_{mm'}$ is a convenient term to describe parity effects, e.g. $s_{mm'} = (1 - (-1)^{m-m'})/2$ to cancel coupling for odd m–m'. In most of the following, we shall assume a constant $\kappa_{mm'} = \kappa$ apart from parity considerations. The next degree of refinement would be to use a slowly varying constant, which would reflect the variations of the diffraction efficiencies of underlying plane waves (see Section 3) at the frequencies of interest.

As for the practical matrix implementation of the CMT, it implies a $2N \times 2N$ matrix, and an indexing rule of its $2N$ elements to connect them with the N forward and N backward modes (canonically either odd elements are forward, even ones being backward, or $1, \ldots, N$ are forward, $N+1, \ldots, 2N$ being backward) [4].

To illustrate this, Fig. 1(c) and (d) compares CMT and exact dispersion relations (obtained by Plane Wave Expansion [PWE]) of a W15 PhC waveguide [1]. The agreement is excellent as regards the coupling scheme, from the fundamental mode region to the whole region of excited modes between fundamental modes and BZE, within the photonic gap. From a mere 2×2 perspective, where the forbidden gap just scales like $\kappa_{11} \equiv \kappa$ [10], it may seem surprising to get, with the same constant, both the smaller gaps and the larger ones at BZE. When several branches are involved, however, the individual gaps have a ''reentrant'' non-monotonous behavior vs. κ, whereby the gap size first increases until it reaches the interband separation and then shrinks again [4]. The intermediate situation is the basis of the critical coupling reviewed in Section 4. The ''flocking'' of multiple bands coupled to other modes can also be grasped from a ''dark mode'' perspective [11].

The curly ''necklace'' branches that emerge around the BZE are characterized by a hyperbolic shape and by the period of their necklace curves (their curls or lobes). Their origin lies in the shape of the ''stripe of minigaps'' [1,3] that arise between the regular net of crossing branches for higher order modes, as shown in Fig. 2(a). Solving for the crossing between mode $m+p$, $\omega_{m+p} = (c/n)^2[k^2 + ((m+p)\pi/W)^2]^{1/2}$ and a folded mode $m' = m - p$, $\omega_{m-p} = (c/n)[(k-2K)^2 + ((m-p)\pi/W)^2]^{1/2}$, and starting from the point of coordinate $(\omega = \omega_m, k = K)$ on, tracking the locus of the successive $p = 1, 2, \ldots$ minigaps results in the following ''stripe dispersion'' relationships:

$$K - k = mp\left(\frac{\pi^2}{W^2}\right)\left(\frac{1}{K}\right) \tag{2}$$

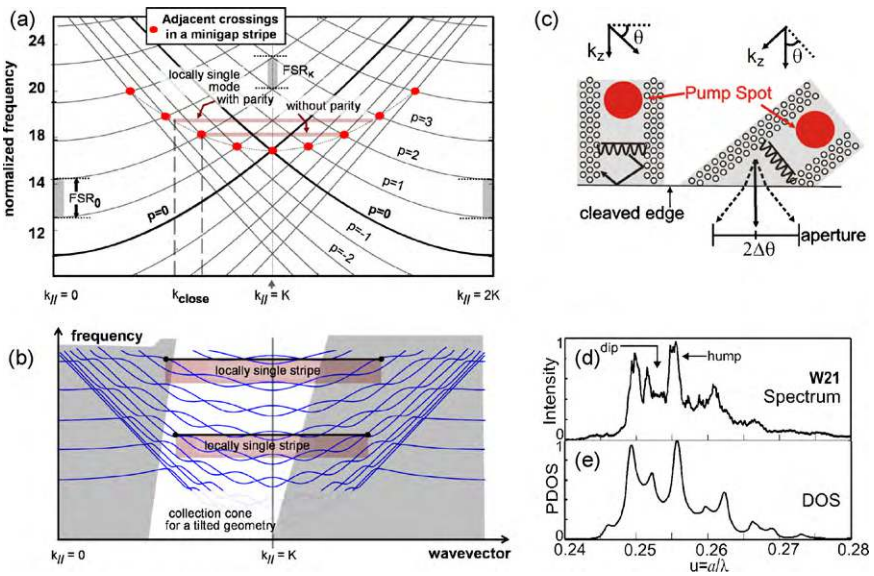

Fig. 2. (a) Crossing of uncoupled modes define minigap stripes; (b) scheme of the structure of collective ''necklace'' slow modes and locally monomode regions; (c) tilted waveguide arrangement to measure the slow modes; (d) luminescence from a W21 waveguide revealing its highly modulated DOS structure for the collected k-range, compared to the exact (2D) DOS model.

$$\omega_{m+p} = \frac{c}{n}\left[\left(K^2 + \frac{m^2\pi^2}{W^2}\right)\left(1 + \frac{p^2\pi^2}{(WK)^2}\right)\right]^{1/2}$$
$$= \omega_m(K) \quad 1 + \frac{p^2\pi^2}{(WK)^2}\Bigg)^{1/2} \tag{3}$$

By substituting for p from Eq. (2) in Eq. (3), the dispersion becomes explicit $\omega(K-k)=\omega_m(K)[1+\{(K-k)W/m\pi\}^2]^{1/2}$. These are the hyperbola describing the stripes (red dots of Fig. 2(a)) and thus the trends of the coupled bands that are constrained between stripes. Their curvature is exactly the same as the initial Fabry–Perot hyperbola $\omega_m(k) = \omega_m(0)[1+\{kW/m\pi\}^2]^{1/2}$ centered at $k = 0$. Note that the coupled branch number is unchanged when following the stripe, but p increments at each lobe of the necklace, a fact hidden in the above form of $\omega(K-k)$, and for which extra indexing efforts are indeed unnecessary. However, there is no parity consideration above, hence factors of two actually relate several quantities between Figs. 1(c) and (d) and 2(a) such as free spectral range.

We give some more scaling rules for these stripes, based on the schemes of Fig. 2(a) and (b): firstly, the local spacing (''free spectral range'') of bands/stripes at K is:

$$\mathrm{FSR}_K = \left(\frac{c}{n}\right)\left(\frac{\pi}{W}\right)\frac{m\pi}{m^2\pi^2 + K^2W^2}$$
$$= \mathrm{FSR}_0\,\frac{m\pi}{(m^2\pi^2 + K^2W^2)^{1/2}} \tag{4}$$

where FSR_0 is the usual Fabry–Perot free range (see [12] for Fabry–Perot type modes in PhC). The reduction ratio ($\mathrm{FSR}_K/\mathrm{FSR}_0 < 1$) is also the ratio of band edge to zone center frequencies, $\omega_m(k = K)$ and $\omega_m(k = 0)$.

With reference to the various illustrations of Fig. 2(a) and (b), the size of k-space where a given hyperbolic branch lies below the next branch is $[K - k_{\mathrm{single}}, K + k_{\mathrm{single}}]$. It is a useful measurement of the effective single-mode domain created by the stripes. Specifically, this k-space range may be derived as follows:

$$\left|K - k_{\mathrm{single}}\right|\frac{a}{\pi} = \left(\frac{a}{W}\right)\left(\frac{2m}{\pi}\right)^{1/2}\left[\frac{\pi m}{(\pi^2m^2 + K^2W^2)^{1/2}}\right] \tag{5}$$

where we formally use the waveguide period a to retain a dimensionless formulation. Hence, the size of this region compared to the Brillouin zone is not as small as the naïve fraction $1/N \sim a/W$ (a small number in a broad waveguide), since it is reinforced by a ''mesoscopic'' factor $(2m/\pi)^{1/2}$. The last factor in square brackets is again $\mathrm{FSR}_K/\mathrm{FSR}_0$, and is typically 0.6–0.8 in our context. A typical value of m is on the order W/a to operate around the first Bragg order of contradirectional coupling. Hence, the quasi-single mode region is fairly larger than the naïve prediction $1/N \sim a/W$: it can occupy ~30% of the Brillouin zone while operating at orders $m = 20$ or so, roughly as occurs in Fig. 1(c) and (d). We can also count the number of lobes of the necklace (or minigaps) within the range $[K - k_{\mathrm{single}}, K]$, based on Eq. (2), since the integer p, which initially counts anticrossings, obviously also counts lobes of the nearby bands. The result reads:

$$p_{\mathrm{single}} = \left(\frac{W}{a}\right)\left(\frac{m\pi}{2}\right)^{-1/2}\left[\frac{\pi m}{(\pi^2m^2 + K^2W^2)^{1/2}}\right] \tag{6}$$

This value is nearly the square root of the total number of lobes in the Brillouin zone (naturally of order W/a) since m is on the order of W/a. In other words, this is a $\sqrt{N}$ scaling. This trend also explains why it is difficult to define a strict boundary for the validity of this description. For narrow waveguides, the number of lobes gently decreases to unity, so that reminiscence of the W15 bandstructure of Fig. 1(c) and (d) can be found in, say, much narrower W2 waveguides, but with $p_{\mathrm{single}} \sim 1$.

The observation of these stripes of minigaps was reported in [3]. The highly structured band diagram translates into a density-of-states (DOS) with ''on-off'' modulation if the proper k-range is collected Fig. 2(c). We provide in Fig. 2(d) and (e) a typical example of a DOS modulation for TE polarization seen through the photoluminescence of a quantum well (centered around $\lambda = 1.5$ μm) in an InP based W21 PhC waveguide. A guide with its axis tilted by 60° to the cleaved edge (Fig. 2c) ensured the sampling of k-space modes in ~30% of the Brillouin zone. This example displays a complex spectrum that was very well reproduced by using a PWE-based density-of-states calculation. In other cases, a more ''on/off'' modulation was seen up to W31. This indicates the possible advantageous use of this phenomenon to better exploit the spontaneous emission inside an open resonator, for instance to extract a given spectral range into selected modes.

3. Littrow lasing and low laser threshold

From the well-known picture of lasing at photonic band edges, we infer that minigap edges may equally privilege stimulated emission [13,14], provided their spectral position falls in the gain region of the guide's active material. They offer several local zero-group velocity points, but the BZE point is the most likely to

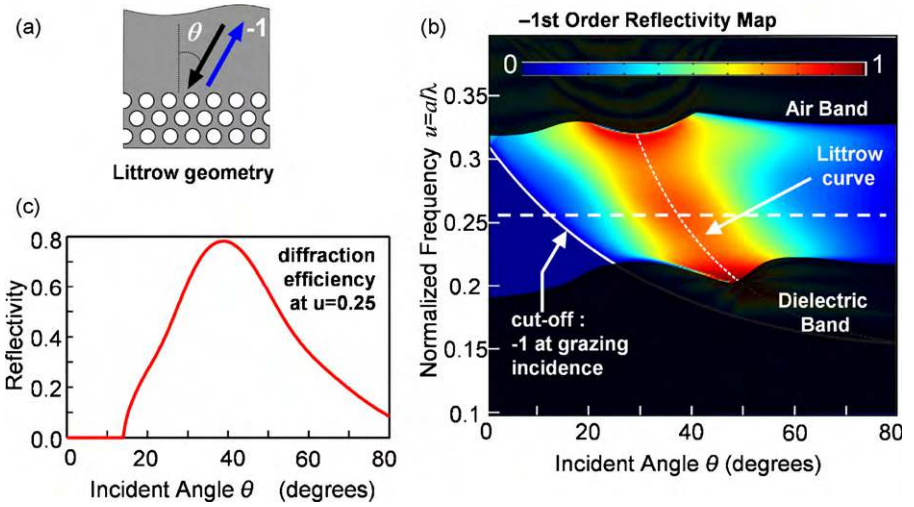

Fig. 3. (a) Littrow diffraction onto a PhC cladding; (b) color map of diffraction efficiency in -1 reflected order, with cut-off curve and Littrow curve for a typical PhC; (c) plot of efficiency for the normalized frequency $u = a/\lambda = 0.25$. (For interpretation of the references to color in this figure legend, the reader is referred to the web version of the article.)

lase. At this BZE point, $k_{||} = \pi/a$, a mode $E_m^+(x,z)$ is reflected into its counterpart $E_m^-(x,z)$. The textbook operation of distributed Feedback (DFB) lasers can be revisited with the scheme of Fig. 4(a) picturing some of the underlying plane waves of $E_m^{\pm}$. Note that the main interaction of Fig. 4a involves wavevectors with two opposite $k_{||}$ -components, because $k_{||} - 2\pi/a = -k_{||}$ (but at variance with DFB lasers, it is not the main component, see [15,16] for some more generality). This is just ''Littrow diffraction'' in optics, an oblique incidence beam diffracted back on its incident path, Fig. 3(a). Backward coupling is thus closely related to diffraction efficiency in (-1) order, which is mapped in Fig. 3(b) for a typical triangular PhC [5], with cut-off curves and Littrow curve. In Fig. 3(c) the diffraction efficiency near mid-gap is plotted.

The free spectral range of stripes, FSR_K for a symmetric guide, separates the pair of branches of the ''necklaces'' (absorbing the two modes $E_m^{\pm}$). The zone-edge FSR is halved only for a nonsymmetric case [1]. Even for a symmetric case, the two branches of a ''necklace'' are not identical, therefore the lasing FSR can differ from the $\omega_m(K)$ pattern.

A ''Littrow laser'' realization was discussed in [5] and relies on distributed Littrow-type back reflection in an open-resonator geometry, shown in Fig. 4(a). We display in Fig. 4(b) and (c) the variation of the spectral pattern for a larger series of injected current values. Above the background related to the $k = 0$ Fabry–Perot mode (collection is on the side of the laser, along the red arrow ''FSR_0'' of the inset), a clear two-moded pattern emerges either at low current or at high current, although it is spoiled in between due to limited gain spectral width (at 150 mA and 200 mA).

As for the reason for a lower lasing threshold for Littrow modes, a sensible comparison can be made with

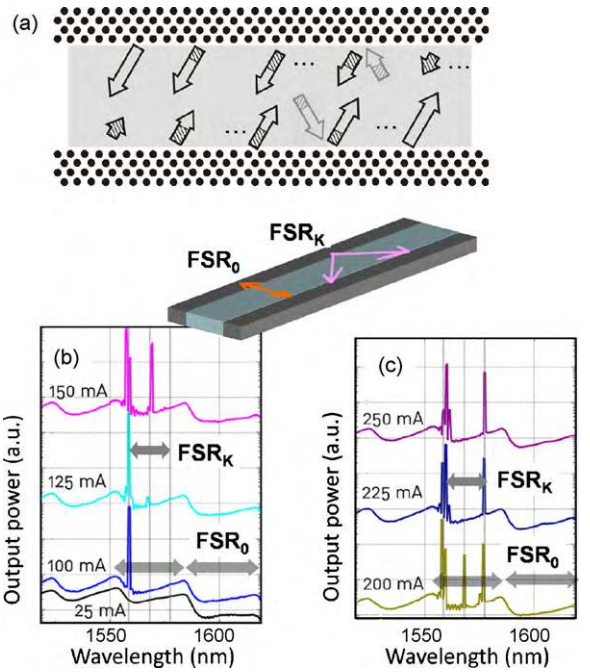

Fig. 4. (a) Distributed feedback revisited for ''Littrow lasing''. The white and hatched fraction of arrows suggest the role of feedback and feed forward waves; (b) and (c) spectra recorded at increasing currents for the laser of Ref. [5], with the two kinds of FSR as signaled, see also the top inset. (For interpretation of the references to color in this figure legend, the reader is referred to the web version of the article.)

Fabry–Perot modes: consider an invariant non-periodic waveguide. Transverse oscillation of Fabry–Perot modes evokes the usual condition $R_1R_2\exp(gW) = 1$ ($W \equiv L$ in usual notations) with R_1 and R_2 the reflectivities and g the spatial gain. For Littrow modes, the round-trip path is longer, $2W/\cos\theta$ instead of $2W$. For a given reflectivity, this lowers the threshold gain by just the $\cos\theta$ factor, which can range from 0.6 to 0.9. Such a lower gain results in much less power consumption and much less heat sink issues for a broad area laser or a gain-clamped semiconductor optical amplifier (GCSOA [17], a useful variant of SOA).

The obtainment of single-transverse-mode Littrow lasing is important in applications, thus the multimode lasing situation of Fig. 4b is detrimental. The option of Fig. 5(a) is a simple solution in the case of PhC waveguides, inspired by the coupled-cavity generic problem. A narrow guide ''W2'' is carved on the side of the main guide. Being narrow, it offers few eigenmodes for coupling from the large cavity to it. At each such eigenmodes, a dip appears in the effective reflectivity as seen from the large guide, see Fig. 5(b), because losses (scattering) occurs mostly on boundaries, which are much more visited: the W2 guide serves as a resonant ''photon dumper''. Two close dips are easily obtained in W2 which displays a ''necklace'' pattern of two branches with the good order of separation (FSR_K of the broad guide) and a modest dispersion at BZE. Alignment of Littrow modes, material gain, and the recovery window of our proposed added waveguide should result in robust monomode operation in these broad waveguides.

4. Critical coupling in broad periodic waveguides

Looking at the pair of branches of a ''necklace'', the group velocity in transmission windows ranges from zero to an upper bound $v_g^{\max} = c/n_g^{\min}$, $n_g^{\min}$ being the lower bound of group index. It is dictated by the width of the miniband and the k-periodicity of the anticrossings. Shrinking this spectral width reduces $v_g^{\max}$. To understand what are the parametric changes to reach such a ''compression'' of photonic bands, let us recourse to CMT, whereby one may conveniently vary this compression through the coupling strength κ. It is simple to tackle in a CMT toy model [4] the evolution of ''spectral width'' of necklace-type bands for fixed FSR_K but variable κ. At low κ, all anticrossings first grow, and the necklace spectral width decreases. But this occurs only until a point where nearby branches, above or below the gap of interest, constrain these growths. At this point, gaps are maximal and the ''spectral width'' is thus minimal. We call this situation the ''critical coupling'' because for stronger coupling strength κ, the stripe of minigaps again shrinks while the spectral width grows again. We obtained a simple result (numerically, but it certainly has a mathematical demonstration), by noting that for any number of equidistant branches, the critical coupling situation is realized when $\kappa \equiv \kappa_c = \mathrm{FSR}_K/\pi$ (remember that in the 2×2 case, a gap of width 2κ is generated, hence the collective aspect of equidistant branches brings a factor $2/\pi$ on the relation between gap and coupling).

Fig. 6 illustrates the relation dispersion near the ''critical coupling'' regime for an ideal system (thanks to the CMT description). We showed [4] that the critical coupling condition is attainable in real systems notably thanks to high-aspect ratio V-groove-type type structures (V-corrugations).

Of course, the large hyperbolic dependence centered on the BZE is unavoidable in our spirit and clearly limits the degree of attainable slow light phenomena. A k-range well inside $[K - k_{\mathrm{single}}, K + k_{\mathrm{single}}]$ is needed to reach the lowest group velocities.

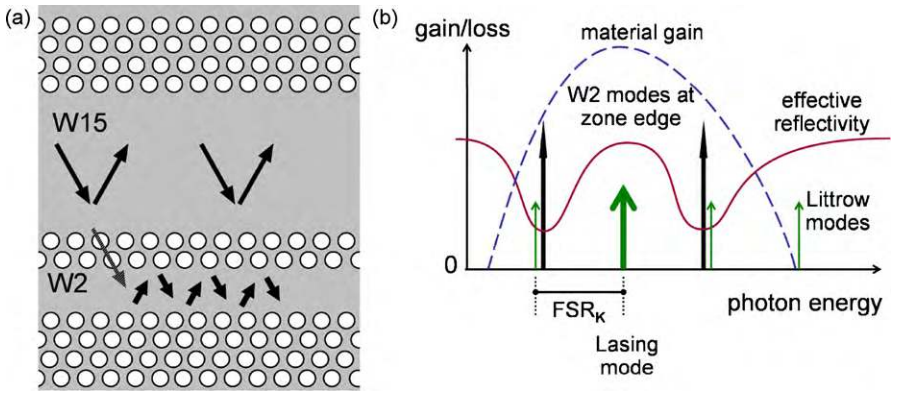

Fig. 5. (a) Broad waveguide coupled to a W2 waveguide through a few rows; (b) loss/gain/reflectivity spectral arrangement to obtain single mode lasing.

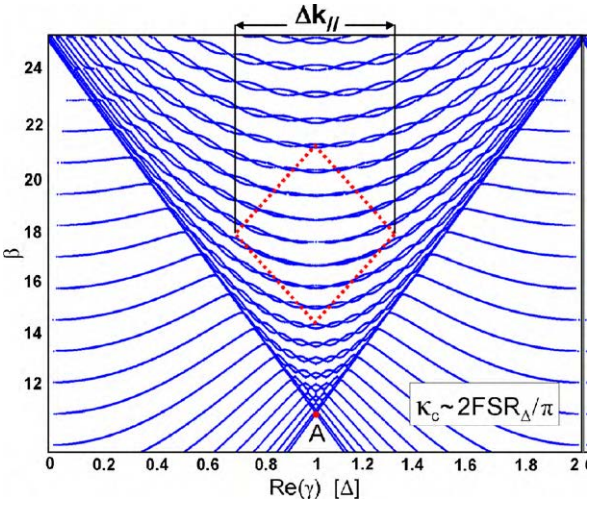

Fig. 6. Coupled mode theory dispersion diagram similar to Fig. 1(a) but with coupling constant tuned to the critical coupling range, attained in the lozenge outlined.

Furthermore, we showed in [1] that a special interest of this understanding of the existence of a critical coupling is the potential to predict "optimally slow" light in a structure, in a typical case where among a number of optogeometric parameters, only one or two can be practically tuned, as sketched in Fig. 7: because the feedback coefficient of "Littrow modes" κ has a close link to an overlap integral between $E_m^{\pm}$ profiles and the periodicity, we may improve the "slowness" of a given structure by applying any recipe that adjusts the overlap so as to obtain critical coupling. The perturbation is, physically, the first Fourier component of the dielectric profile taken along a line x, $\hat{\varepsilon}_{\pm 1}(x) \equiv \int \varepsilon(x,z)\ \exp(iG_{\pm 1}z)\ dz$. Once a sufficiently

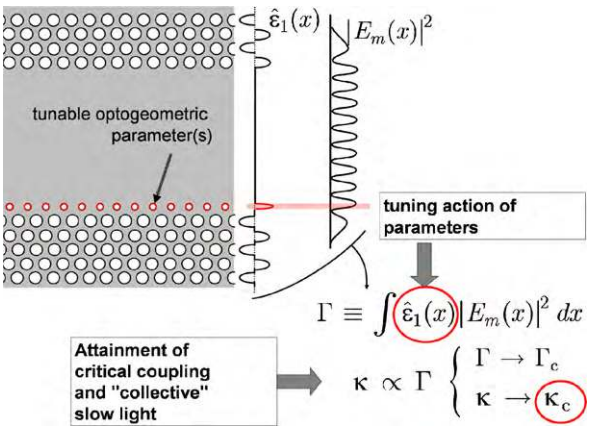

Fig. 7. Graphical outline of the recipe in Ref. [1] to attain critical coupling by tuning any available optogeometric parameter through the perturbation integral Γ.

monotonous relation exists between the coupling strength κ and the parameter controlling $\varepsilon(x, z)$, e.g. the depth of a corrugation, the size or position of a hole, or its refractive index, then, reaching an optimally slow waveguide design amounts to tune this specific parameter until κ attains the critical value (Fig. 7).

A few examples were chosen to illustrate this approach in [1] for the case of photonic crystal waveguides in the so-called TE polarization.

Another aspect of critical coupling was seen recently when shaping a section of a corrugated waveguide as an open resonator [2]. The resonator design reaches a maximum quality factor Q at the critical coupling regime as well, as could be expected: a nearly dispersionless situation is reached when modes are best localized, as happens in the CROW (Coupled Resonator Optical Waveguide) context [18,19] for very weakly coupled resonators.

We also attempted to draw two connections of this critical coupling regime to neighbor scientific domains, namely graphene nanoribbons [20] and "dark states"[11].

In the case of graphene nanoribbons, the dispersion relation of electrons in graphene is linear around the pseudogap. Therefore, a graphene nanoribbon (GNR) resembles a broad optical waveguide [20]. Edge states that are present e.g. in zig–zag GNR may also have a counterpart in optics, as illustrated recently [21] around the concept of one-way waveguides [22], but this is not our main point. Our analogy indicates the possible slow down of electrons by a proper edge corrugation [20] and thus the formation of an open electron resonator, similar to the optical one in [2]. One might ask why is there any interest in slowing down the pleasantly "fast" electrons of graphene or "spoil" their mobility. The answer is much as in optics: when you have a low loss system, you try to build the best Fabry–Perot or micro-ring from it to further exploit its coherent nature and its particular high or low sensitivity to various factors. Also, it is hard to coherently get electrons out of graphene, e.g. across a tunnel barrier through a foreign material, without being at high risks at the interface due to its possible local (chemical) modifications, defect tunneling, etc. Relying on reflections seems therefore a better option. It remains to be seen what progresses can be made through field effect and electrodes to manipulate electrons in graphene to elaborate on this strategy, of course.

As for the connection with "dark states", it emerged [11] because the simplest CMT modeling initially performed on "critical coupling", involving linear branches, revealed the appearance of two "bright" states and $2N - 2$ "dark states" when coupling $N + N$

states beyond critical coupling. Above the critical coupling regime, most of the coupled modes are formed by the hybridization of one of the underlying modes with its nearest (energy) neighbors in such a way that a high exchange of amplitude can take place without a high energy shift of the bands, as appears analytically when discussing the simpler $1 \times N$ coupling scheme [11,23].

To conclude this part, we note that Longhi's results [24] on optical analogy of quantum phenomena are also very interesting. They have been mostly elaborated, however, in the context of directional rather than contradirectional coupling, which entails clear differences.

5. Conclusion

Broad waveguides with periodic edges offer more structured features than might be thought from the N^{-1} scaling of DOS features in invariant (non periodic) waveguides. A $N^{-1/2}$ scaling emerges for the fraction of Brillouin Zone still displaying large DOS modulation. The so-called Littrow modes forming in these systems have been seen to be promising candidates in broad-area lasers. Finally, the critical coupling condition has been illustrated and some more profound physical consequences briefly mentioned, on graphene nanoribbons and on dark states.

Acknowledgments

This work was carried out in the framework of the CNano IdF ''POLYKAPPA'' project. The author is indebted to R. Brénot and G.H. Duan for their help at III–V Lab on the lasing measurements.

References

[1] O. Khayam, H. Benisty, General recipe for flatbands in photonic crystal waveguides, Opt. Express 17 (2009) 14634–14646.
[2] H. Benisty, Single-material coupling-tolerant semi-planar microresonator using Littrow diffraction, Photon. Nanostruct. Fund. Appl. 7 (2009) 115–127.
[3] O. Khayam, H. Benisty, C. Cambournac, Experimental observation of minigap stripes in periodically corrugated broad photonic wires, Phys. Rev. B 78 (4) (2008) 153107.
[4] H. Kurt, H. Benisty, T. Melo, O. Khayam, C. Cambournac, Slow-light regime and critical coupling in highly multimode corrugated waveguides, J. Opt. Soc. Am. B 25 (2008) C1–C14.
[5] O. Khayam, C. Cambournac, H. Benisty, M. Ayre, H. Brenot, G.H. Duan, W. Pernice, In-plane Littrow lasing of broad photonic crystal waveguides, Appl. Phys. Lett. 91 (1–3) (2007) 041111.
[6] H. Benisty, C. Weisbuch, Photonic crystals, in: E. Wolf (Ed.), Progress in Optics, vol. 49, Elsevier, Amsterdam, 2006, pp. 177–315.
[7] H. Benisty, C. Weisbuch, D. Labilloy, M. Rattier, C.J.M. Smith, T.F. Krauss, R.M. De La Rue, R. Houdré, U. Oesterle, D. Cassagne, Optical and confinement properties of two-dimensional photonic crystals, IEEE J. Lightwave Technol. 17 (1999) 2063–2077.
[8] J.D. Joannopoulos, R.D. Meade, J.N. Winn, Photonic Crystals, Molding the Flow of Light, Princeton University Press, Princeton, NJ, 1995.
[9] S. Olivier, H. Benisty, C. Weisbuch, C.J. Smith, T.F. Krauss, R. Houdré, Coupled-mode theory and propagation losses in photonic crystal waveguides, Optics Express 11 (2003) 1490–1496.
[10] A. Yariv, Quantum Electronics, 2nd ed., John Wiley & Sons, New York, 1975.
[11] H. Benisty, Dark modes, slow modes, and coupling in multimode systems, J. Opt. Soc. Am. B 26 (2009) 718–724.
[12] M. Rattier, H. Benisty, C.J.M. Smith, A. Béraud, D. Cassagne, T.F. Krauss, C. Weisbuch, Performance of waveguide-based two-dimensional photonic-crystal mirrors studied with Fabry–Pérot resonators, IEEE. J. Quantum Electron. 37 (2001) 237–243.
[13] E. Viasnoff-Schwoob, C. Weisbuch, H. Benisty, S. Olivier, R. Houdré, C.J.M. Smith, Spontaneous emission enhancement at a photonic wire miniband edge, Opt. Lett. 30 (2005) 2113–2115.
[14] E. Viasnoff-Schwoob, C. Weisbuch, H. Benisty, S. Olivier, S. Varoutsis, I. Robert-Philip, R. Houdré, C.J.M.S. Smith, Spontaneous emission enhancement of quantum dots in a photonic crystal wire, Phys. Rev. Lett. 95 (2005) 183901.
[15] D.B. Burckel, S.J.R. Brueck, Generalized transverse Bragg waveguides, Opt. Express 13 (2005) 9202–9210.
[16] L. Zhu, A. Scherer, A. Yariv, Modal gain analysis of transverse bragg resonance waveguide lasers with and without transverse defects, IEEE J. Quantum Electron. 43 (2007) 934–940.
[17] J. Sun, G. Morthier, R. Baets, Numerical and theoretical study of the crosstalk in gain clamped semiconductor optical amplifiers, IEEE J. Sel. Top. Quantum Electron. 3 (1997) 1162–1167.
[18] A. Yariv, Y. Xu, R.K. Lee, A. Scherer, Coupled-resonator optical waveguide: a proposal and analysis, Opt. Lett. 24 (1999) 711–713.
[19] S. Olivier, C. Smith, M. Rattier, H. Benisty, C. Weisbuch, T. Krauss, R. Houdré, U. Oesterle, Miniband transmission in a photonic crystal coupled-resonator optical waveguide, Opt. Lett. 26 (2001) 1019–1021.
[20] H. Benisty, Graphene nanoribbons: photonic crystal waveguide analogy and minigap stripes, Phys. Rev. B 79 (2009) 155409.
[21] X. Ao, Z. Lin, C.T. Chan, One-way edge mode in a magneto-optical honeycomb photonic crystal, Phys. Rev. B 80 (4) (2009) 033105.
[22] Z. Wang, Y. Chong, J.D. Joannopoulos, M. Soljacic, Observation of unidirectional backscattering-immune topological electromagnetic states, Nature 461 (2009) 772–776.
[23] R. Houdré, R.P. Stanley, M. Ilegems, Strong coupling régime in the presence of inhomogeneous broadening: resolution of an homogeneous linewidth in an inhomogeneously broadened system, Phys. Rev. A 53 (1996) 2711–2715.
[24] S. Longhi, Quantum-optical analogies using photonic structures, Laser Photon. Rev. 3 (2009) 243–261.